Electron paramagnetic resonance study of the multisite character of Yb^{3+} ions in $LuVO_4$ single crystals

2005 J. Phys.: Condens. Matter 17 3061

(http://iopscience.iop.org/0953-8984/17/19/019)

INSTITUTE OF PHYSICS PUBLISHING JOURNAL OF PHYSICS: CONDENSED MATTER

J. Phys.: Condens. Matter **17** (2005) 3061–3072 doi:10.1088/0953-8984/17/19/019

Electron paramagnetic resonance study of the multisite character of Yb^{3+} ions in $LuVO_4$ single crystals

O Guillot-Noël[1,4], Ph Goldner[1], M Bettinelli[2] and E Cavalli[3]

[1] Ecole Nationale Supérieure de Chimie de Paris (ENSCP), Laboratoire de Chimie Appliquée de l'Etat Solide, UMR-CNRS 7574, 11 rue Pierre et Marie Curie, 75231 Paris Cedex 05, France
[2] Dipartimento Scientifico e Tecnologico and INSTM, Università di Verona, Ca' Vignal, Strada Le Grazie 15, 37134 Verona, Italy
[3] Instituto Nazionale per la Fisica della Materia e Dipartimento di Chimica Generale ed Inorganica, Chimica Analitica e Chimica Fisica, Università di Parma, Viale delle Scienze, 43100 Parma, Italy

E-mail: olivier-guillotn@enscp.fr

Received 23 February 2005, in final form 7 April 2005
Published 29 April 2005
Online at stacks.iop.org/JPhysCM/17/3061

Abstract

Electron paramagnetic resonance (EPR) is used to identify the different substitution sites of Yb^{3+} ions in the $LuVO_4$ host. Three different types of sites are observed. One site, referred to as Yb_I, with tetragonal D_{2d} symmetry characterized by g-values of $|g_\perp| = 0.59(7)$ and $|g_\parallel| = 6.464(9)$, corresponds to 80% (50%) of the total number of Yb^{3+} ions for the 1% (5%) doped compound. Two other tetragonal sites, referred to as $Yb_{IIa,IIb}$, with the same D_{2d} symmetry and characterized by g-values of $|g_\perp| = 0.89(3)$, $|g_\parallel| = 2.75(1)$ and $|g_\perp| = 0.89(3)$, $|g_\parallel| = 2.84(1)$, represent 20% (50%) of the total number of ytterbium ions for the 1% (5%) compound. One minor site, referred to as Yb_{III}, corresponding to less than 1% of the Yb^{3+} ions, with a lower C_{2v} or D_2 symmetry, is also seen in the EPR spectra. The temperature dependence of the EPR linewidth is studied and shows for all the sites a dominant Orbach process for the spin–lattice relaxation time T_1 for $T > 12$ K.

1. Introduction

Rare earth doped orthovanadate crystals and in particular orthovanadates such as YVO_4 and $GdVO_4$ doped with Nd^{3+} ions are well known solid state laser materials [1]. Recently, laser oscillation in ytterbium doped $GdVO_4$ [2] and YVO_4 [3] has also been demonstrated. These materials are especially interesting for high power laser applications because of the low quantum defect of ytterbium and the high thermal conductivity of the vanadates.

[4] Author to whom any correspondence should be addressed.

$LuVO_4$:Yb^{3+} should exhibit similar properties with the additional advantage of a very small mass difference between Yb^{3+} and Lu^{3+}, which allows high doping without decreasing the thermal conductivity [4].

Moreover, it has been shown repeatedly in the past that lutetium containing crystals doped with trivalent rare earth ions (Ln^{3+}) are characterized by better spectroscopic and laser properties with respect to the corresponding yttrium containing materials. For example, the fluorescence efficiencies of Pr^{3+} and laser performances of Ce^{3+} are higher in $LiLuF_4$ and $LuPO_4$ than in $LiYF_4$ and YPO_4 [5, 6]. In the specific case of zircon-type vanadates, neodymium absorption and emission cross sections (at 809 and 1066 nm, respectively) have been reported to be higher in $LuVO_4$ than for YVO_4 [7]. The reasons for this behaviour have not been fully ascertained; however, explanations based on different crystal field splittings of the Ln^{3+} manifolds [8] and on the location of the lutetium 4f levels at the top of the valence band [9] have been proposed in the literature. It is reasonable to expect that a similar behaviour is found for $LuVO_4$:Yb^{3+}.

$LuVO_4$ crystallizes in the zircon type structure and belongs to the tetragonal $I4_1/amd$ space group. The lattice parameters of $LuVO_4$ are $a = 7.0254(1)$ Å and $c = 6.2347(1)$ Å [10]. Yb^{3+} ions substitute eightfold coordinated Y^{3+} ions, forming [YO_8] bisdisphenoids with D_{2d} point site symmetry. The eight oxygen ions are grouped in two sets differing by the Lu–O bond lengths with four long bonds of 2.4108(7) Å corresponding to oxygen shared with VO_4 tetrahedra and four shorter bonds of 2.2511(6) connected with the other bisdisphenoids [10]. Despite the simple zircon-type structure, which allows only one substitution site for rare earth ions, several previous studies performed on neodymium doped YMO_4 crystals with M = V, P and As reveal a multisite character for the rare earth ions [11]. This multisite behaviour leads to several additional lines in the optical spectra [12]. The interpretation of their origin is of fundamental interest if one wants to optimize the laser properties of such crystals.

The purpose of the present work is to analyse the multisite character of ytterbium ions in the $LuVO_4$ host by electron paramagnetic resonance spectroscopy (EPR). EPR spectroscopy is a powerful tool to identify a paramagnetic ion in different sites. The g-factor of a metal is closely related to the wavefunction of the electronic ground state and therefore depends not only on the spin–orbit coupling but also on the point symmetry of the crystallographic site. The sensitivity of EPR to local symmetry is such that ions in sites with slightly different symmetries give EPR spectra with well defined resonance lines. Previous EPR study of Yb^{3+} ions in $LuVO_4$ [13] did not mention the multisite character of ytterbium; only the g-factor and the principal values of the magnetic hyperfine interaction were given.

2. Experimental details

Yb^{3+} doped $LuVO_4$ single crystals were grown by spontaneous nucleation from a $Pb_2V_2O_7$ flux in the 1300–900 °C temperature range [14]. Reagent grade PbO, V_2O_5 and Lu_2O_3 in suitable ratios were used as starting materials. The doping was achieved by adding Yb_2O_3 to the growth batch: crystals with 1% and 5% nominal molar concentrations of Yb^{3+} with respect to Lu^{3+} were synthesized. A small amount of $Na_2B_4O_7$ was added as flux modifier, allowing us to obtain good quality crystals up to $5 \times 2 \times 1$ mm^3 in size, elongated in the direction of the crystallographic c axis [15].

EPR measurements were performed between 4.5 and 25 K with a X-band (9.5 GHz) Bruker ELEXSYS E 500 spectrometer equipped with a variable temperature accessory from Oxford Instruments. The crystals were mounted on a small Perspex sample holder to allow their orientation with respect to the magnetic field. For a paramagnetic centre in a single crystal, the g-factor is a three by three matrix. The determination of the principal g values and

the director cosines of the principal tensor axes with respect to a reference axis set is obtained from the angular variations of the experimental g factor in three orthogonal crystal planes, e.g. the crystallographic (001), (010) (100) planes. For example, in the (001) plane, starting from the a axis, the angular variation of the g-factor is given by the following equation [16]:

$$g^2(\theta) = g_{aa}^2 \cos^2(\theta) + g_{bb}^2 \sin^2(\theta) + 2g_{ab}^2 \sin(\theta)\cos(\theta) \tag{1}$$

where θ is the angle between the magnetic field and the a axis. From the angular variations of the magnetic field in the three (001), (010) (100) orthogonal planes, the following matrix representing the g^2 tensor elements in the (abc) axis system can be generated:

$$(g^2) = \begin{pmatrix} g_{aa}^2 & g_{ab}^2 & g_{ac}^2 \\ g_{ab}^2 & g_{bb}^2 & g_{bc}^2 \\ g_{ac}^2 & g_{bc}^2 & g_{cc}^2 \end{pmatrix}_{(abc)} . \tag{2}$$

Diagonalization gives the principal g-values and their director cosines with respect to the (abc) axis system. These angular variations were obtained by rotating the crystal by steps of 5 or 10° around reference axes with an ≈2° accuracy for crystal orientation.

3. Results and discussion

Free Yb^{3+} ion has a $4f^{13}$ configuration with a $^{2S+1}L_J = {}^2F_{7/2}$ ground state and a $^2F_{5/2}$ excited state at around 10 000 cm^{-1}. S, L, J are the spin, orbital and total momenta, respectively. In a crystal field of D_{2d} symmetry, the $J = 7/2$ level splits into four Kramers doublets (KDs) $|M_J| = 7/2, 5/2, 3/2$ and $1/2$, M_J being the z-component of J. Since only the lowest doublet is populated at liquid helium temperature, the system can thus be described by a fictitious spin $S = 1/2$. Ytterbium has five even isotopes, ^{168}Yb, ^{170}Yb, ^{172}Yb, ^{174}Yb and ^{176}Yb, with nuclear spins $I = 0$ and a total natural abundance of 69.58%, and two odd isotopes, ^{171}Yb with nuclear spin $I = 1/2$ (natural abundance 14.3%) and ^{173}Yb with nuclear spin $I = 5/2$ (natural abundance 16.12%). The EPR spectrum of Yb^{3+} is expected to be composed of an intense central line due to the even isotopes and a hyperfine pattern composed of two sets of $2I + 1 = 2$ and 6 lines for the two odd isotopes with intensities proportional to their natural abundances. As the first excited multiplet $^2F_{5/2}$ of Yb^{3+} is at 10 000 cm^{-1} from the ground multiplet $^2F_{7/2}$, we can assume that the ground state KDs is a pure $J = 7/2$ doublet, i.e. the J-mixing can be neglected.

The EPR spectra of ytterbium-doped $LuVO_4$ are composed of four types of signal (figures 1 and 2). One signal with its hyperfine structure referred to as Yb_I is seen in the 50–150 mT range when the magnetic field is parallel to the c axis (figure 1). Two other signals are also present around 230 mT. As will be shown below, these paramagnetic centres are attributed to Yb^{3+} ions in axial sites; they will be referred to as $Yb_{IIa,IIb}$ (figure 1). Two very weak signals with their hyperfine structure are observed in the 100–300 mT range when the magnetic field is in the (001) plane (figure 2). They are only seen clearly in the (001) plane because for this orientation the Yb_I signal is at high fields and does not hide these weak signals. They will be referred to as Yb_{III} in the following. The relative concentrations of each Yb^{3+} site, measured by double integration of the signals, is found to be 80% (50%) for Yb_I, 20% (50%) for both Y_{IIa} and Yb_{IIb} and less than 1% for Yb_{III} for the 1% (5%) doped $LuVO_4$ single crystals.

3.1. EPR signal referred to Yb_I

The principal signal referred to as Yb_I is attributed to Yb^{3+} in a tetragonal site with D_{2d} point symmetry. Figure 3 shows the angular variations of g^2 of Yb_I in the (100) or (010) planes and

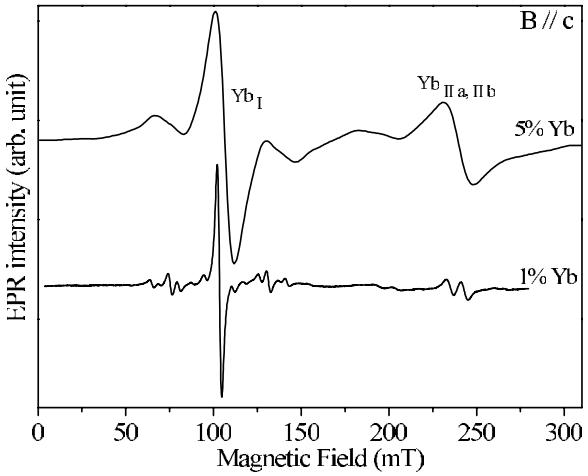

Figure 1. EPR spectra at 6.5 K of 1% and 5% Yb^{3+} in $LuVO_4$ with the magnetic field parallel to the c axis. Three different ytterbium sites are seen: Yb_I, Yb_{IIa} and Yb_{IIb}. The spectra are recorded at 9.5 GHz with a microwave power of 20 mW.

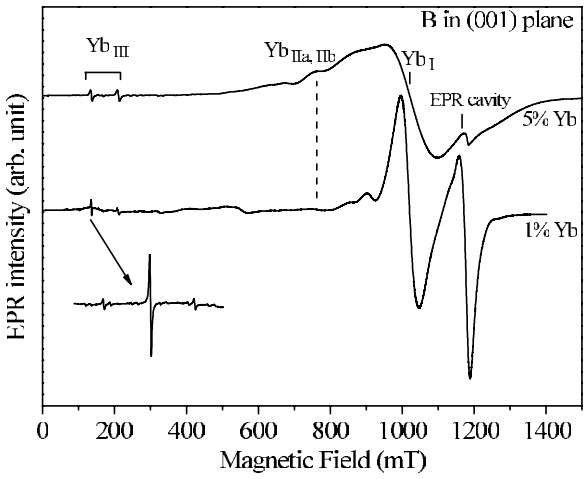

Figure 2. EPR spectra at 6.5 K of 1% and 5% Yb^{3+} in $LuVO_4$ with the magnetic field in the (001) plane. A fourth ytterbium site Yb_{III} is seen. Yb_{IIa} and Yb_{IIb} are hidden by the strong Yb_I EPR signal. The spectra are recorded at 9.5 GHz with a microwave power of 20 mW.

in the (001) plane. The spectrum is invariant in the (001) plane. The angular variations in the (100) or (010) planes are identical and present two extrema when the magnetic field is parallel to the (a or b) and c axes. These features reflect the axial symmetry of the EPR signal which can be described by the following spin Hamiltonian:

$$H = g_{\parallel}\beta B_z S_z + g_{\perp}\beta(B_x S_x + B_y S_y) + A_{\parallel} I_z S_z + A_{\perp}(I_x S_x + I_y S_y) \tag{3}$$

with $S = 1/2$ and $I = 0$ $(5/2)$. No quadrupole interaction is included as we do not see any effect of this interaction in our EPR spectra.

The spin-Hamiltonian parameters $g_{\parallel}$ and $g_{\perp}$ are determined by fitting the experimental angular variations of the central EPR line using equation (1). The principal axes of the g-tensor are found to be parallel to the crystallographic axes and the principal g-values are

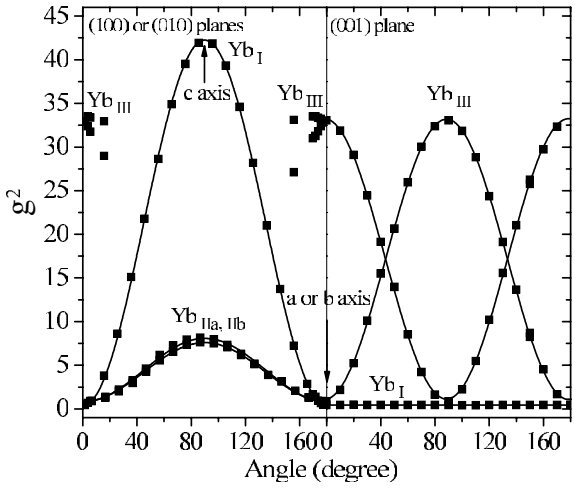

Figure 3. Experimental and simulated angular variation of g^2 in the (100) or (010) planes and in the (001) plane for Yb_I, $Yb_{IIa,IIb}$ and Yb_{III} sites. In the (100) or (010) planes, for a large portion of the angular variation, the Yb_{III} EPR signal is hidden below the Yb_I signal.

$|g_{x,y} = g_\perp| = 0.59(7)$ and $|g_z = g_\parallel| = 6.464(9)$. This result agrees well with the g-values of Yb^{3+} found in [13]: $|g_{x,y} = g_\perp| = 0.59(4)$ and $|g_z = g_\parallel| = 6.482(8)$.

The angular variations of the hyperfine interaction exhibit the same axial symmetry with the principal $A_\parallel$ component parallel to the c axis. The best hyperfine resolution is observed on the EPR spectrum with the magnetic field parallel to the c axis (figure 1), with a linewidth of 2.6 mT for the central line of the 1% doped compound. When the magnetic field rotates from the c axis to the direction of the (001) plane, the lines broaden with a linewidth of 50 mT for the central line and the hyperfine pattern is not seen any more (figure 2). This inhomogeneous broadening is seen at high fields as small g-factor variations are well resolved in the high magnetic field part of the EPR spectra. Therefore, it is only possible to determine the $A_\parallel$ component by fitting the experimental spectrum with the magnetic field parallel to the c axis. The experimental and simulated spectra are gathered in figure 4. The central fields of the hyperfine pattern for both isotopes are slightly shifted to low field from the intense central line and the separations between adjacent hyperfine lines are not strictly equal. These features can be explained by a small second order effect of the hyperfine interaction. From the simulation, we obtain $|A_\parallel^{171}| = 5100$ and $|A_\parallel^{173}| = 1390$ MHz. These hyperfine values are in agreement with the previous measurements of [13] with $|A_\parallel^{171}| = 5196$ MHz. $|A_\parallel^{173}| = 1439$ MHz. The ratio of the hyperfine parameters of the ^{171}Yb and ^{173}Yb isotopes $|A_\parallel^{171}|/|A_\parallel^{173}| = 3.67$ is close to the ratio of the nuclear magnetic moments, equal to -3.63. Weak lines indicated by stars in figure 4 are not explained by the hyperfine pattern. They could be due to either quadrupole transitions or unknown impurities.

As we can neglect the J-mixing between the two $^2F_{7/2}$ and $^2F_{5/2}$ multiplets, we have the following relationship between the spin-Hamiltonian parameters [17]:

$$\frac{g_\parallel}{g_\perp} = \frac{A_\parallel}{A_\perp}. \tag{4}$$

From equation (4) and the previous spin-Hamiltonian parameters, we deduce the perpendicular component of the hyperfine tensor: $|A_\perp^{171}| = 465$ MHz and $|A_\perp^{173}| = 127$ MHz.

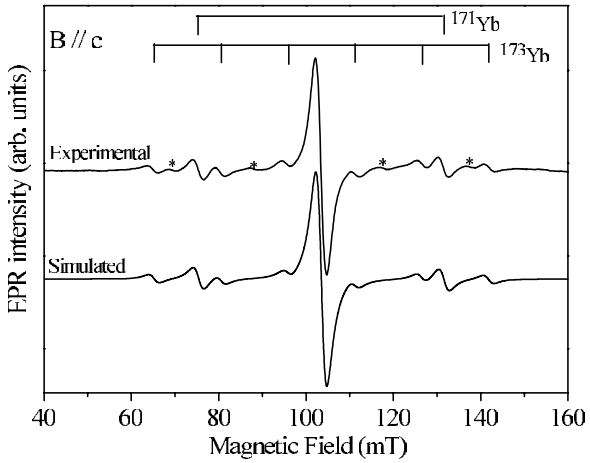

Figure 4. Experimental and simulated EPR spectra at 6.5 K of the Yb_I site with the magnetic field parallel to the *c* axis. The stars indicate unidentified lines which can be due to forbidden transitions or unknown impurities.

Since the crystal field is axial with D_{2d} point symmetry, two irreducible representations Γ_6 and Γ_7 of this group are used to label the KDs of Yb^{3+} ions. Moreover, as we are working in a pure $J = 7/2$ state, the following wavefunctions are obtained for each irreducible representation, where they are expressed in the $|4f^{13}LSJM_J\rangle$ basis set hereafter noted $|J, M_J\rangle$:

$$|\pm\rangle = p\left|\tfrac{7}{2}, \pm\tfrac{7}{2}\right\rangle + q\left|\tfrac{7}{2}, \mp\tfrac{1}{2}\right\rangle \tag{5}$$

$$|\pm\rangle = p\left|\tfrac{7}{2}, \pm\tfrac{5}{2}\right\rangle + q\left|\tfrac{7}{2}, \mp\tfrac{3}{2}\right\rangle \tag{6}$$

for Γ_7 and Γ_6, respectively. By using the general expressions of the g-factor in an axial site, $g_\parallel = 2g_J\langle+|J_z|+\rangle$, $g_\perp = g_J\langle+|J_+|-\rangle$ [17] with $g_J = \frac{8}{7}$ for the $^2F_{7/2}$ multiplet and the normalization condition of the wavefunction, the $g_\parallel$, $g_\perp$ values and the p, q coefficients are related by the following equations:

$$\text{for } \Gamma_7: \quad \begin{aligned} g_\parallel &= \pm g_J\left(7p^2 - q^2\right) \\ g_\perp &= \pm 4q^2 g_J \\ 1 &= p^2 + q^2 \end{aligned} \tag{7}$$

and

$$\text{for } \Gamma_6: \quad \begin{aligned} g_\parallel &= \pm g_J\left(5p^2 - 3q^2\right) \\ g_\perp &= \pm 4\sqrt{3}pqg_J \\ 1 &= p^2 + q^2. \end{aligned} \tag{8}$$

Alternatively, equations (7) and (8) give the following relationship between $g_\parallel$ and $g_\perp$:

$$\text{for } \Gamma_7: \; g_\parallel = \pm 7g_J \pm 2g_\perp \qquad \text{or} \qquad g_\parallel = \pm 7g_J \mp 2g_\perp \tag{9}$$

and

$$\text{for } \Gamma_6: \; 4g_\perp^2 = 45g_J^2 \pm 6g_\parallel g_J - 3g_\parallel^2. \tag{10}$$

To determine the wavefunction associated with the ground state of Yb_I in $LuVO_4$, equations (9) and (10) are plotted in figure 5 together with the experimental values of the g-factor. The g-factor associated with Yb_I does not coincide with the Γ_6 wavefunction and is

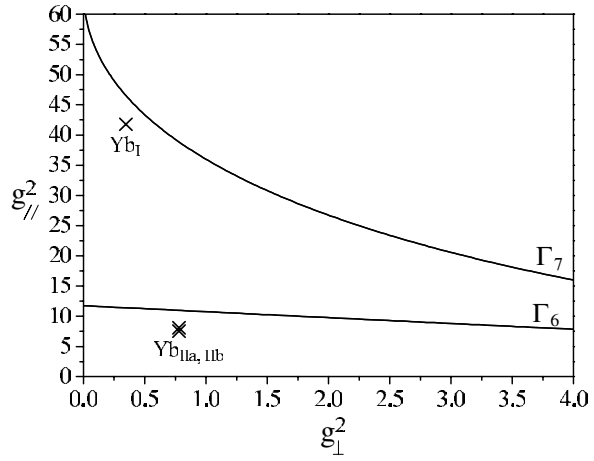

Figure 5. $g^2_\parallel = f(g^2_\perp)$ from equations (9) and (10). The crosses correspond to the experimental $(g^2_\parallel, g^2_\perp)$ points for the Yb_I and $Yb_{IIa,IIb}$ sites.

very close to the Γ_7 irreducible representation. The g-values are calculated to be $|g_\perp| = 0.59$ and $|g_\parallel| = 6.82$ using equations (7) with $|p| = 0.933$ and $|q| = 0.359$. The sign of p and q cannot be determined as the signs of the g-values are not known. The small discrepancies between the calculated g-values and the experimental one (5% for the $g_\parallel$ component) could be explained by a small degree of covalent bonding [18] and/or by orbit–lattice interactions [19], which can be taken into account by considering a orbital reduction factor k such that the orbital momentum L is replaced by kL. This type of wavefunction has been already found for Yb^{3+} in a tetragonal site in CaO [20], $KMgF_3$ [21], and in the zircon type structure YVO_4 [22] and $HfSiO_4$ [23].

The Yb_I EPR line disappears above 20 K, which is the consequence of the lifetime broadening effect produced by the rapid decrease of the spin–lattice relaxation time T_1 at high temperature [17]. Figure 6 gathers the peak-to-peak linewidth Γ of the Yb_I central line versus the reciprocal temperature for the two studied concentrations (1% and 5%) with the magnetic field parallel to the c axis. These variations can be simulated by a dominant Orbach process for the spin–lattice relaxation T_1 given by [17]

$$\Gamma = A + C(\Delta E)^3 \exp\left(-\frac{\Delta E}{k_B T}\right) \tag{11}$$

where k_B is the Boltzmann constant and ΔE is the splitting between the two electronic states involved in the Orbach mechanism, which is in our case the splitting between the ground state and the first excited KDs. A is the temperature independent inhomogeneous broadening which gives a Gaussian lineshape to the EPR line. At very low temperature (8 K) the EPR lineshape is Lorentzian, which means that the broadening is already homogeneous. For both concentrations, we found $\Delta E = 105(10)\,cm^{-1}$, $A = 3.0(3)$ and 10.8(1) mT and $C = 0.024(1)$ and $0.021(1)\,mT/cm^{-3}$ for the 1% and 5% doped compound, respectively.

3.2. EPR signal referred to $Yb_{IIa,IIb}$

Two other signals are seen around 230 mT when the magnetic field is parallel to the c axis (figure 1). It is difficult to follow these lines when the magnetic field is rotated from the c axis towards the a and b axes because they are superimposed on the Yb_I signal (figure 2). However,

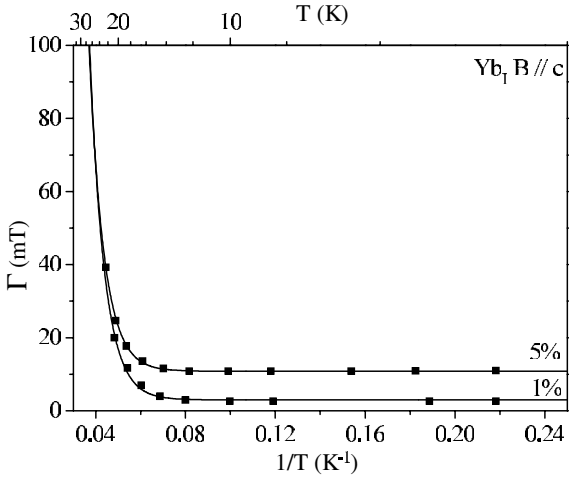

Figure 6. Temperature dependence of the peak-to-peak linewidth Γ of the Yb_I EPR line for two Yb^{3+} concentrations (1 and 5%) with the magnetic field parallel to the *c* axis. The solid curves are calculated with an Orbach process.

the angular variations in the (100) and (010) planes seem to be identical (figure 3). Moreover, in the (001) plane, these signals seem to be invariant under rotation of the magnetic field. The paramagnetic centres responsible for these signals are thus considered to be located on a site of axial symmetry with the principal *g*-factor values parallel to the crystallographic axis. As we show in the following, these lines can be attributed to ytterbium ions and they are referred to as Yb_{IIa} and Yb_{IIb}. From the simulations of the angular variations, the following experimental *g*-factor values are found: $|g_\perp| = 0.89(3)$, $|g_\parallel| = 2.75(1)$ for Yb_{IIa} and $|g_\perp| = 0.89(3)$, $|g_\parallel| = 2.84(1)$ for Yb_{IIb}.

These lines become undetectable above 20 K. This feature is the indication of a short spin–lattice relaxation time comparable to that of the Yb_I site and shows that they are due to rare earth ions. As these lines are easily detected, the associated rare earth ions exhibit the Kramers degeneracy and thus possess an odd number of electrons: they may be the Ce^{3+} (f^1), Nd^{3+} (f^3), Sm^{3+} (f^5), Eu^{2+}, Gd^{3+}, Tb^{4+} (f^7), Dy^{3+} (f^9), Er^{3+} (f^{11}) and Yb^{3+} (f^{13}) ions. We can eliminate the rare earth ions with f^7 configuration because they have zero orbital momentum in the ground state (^{8}S term) and thus are characterized by a long T_1, which makes them detectable at room temperature. We can also eliminate the Nd^{3+} and Er^{3+} ions. Indeed, from [13], these ions are characterized by the following *g*-values: $|g_\perp| = 2.555(4)$, $|g_\parallel| = 0.52(2)$ for Nd^{3+} and $|g_\perp| = 6.86(3)$, $|g_\parallel| = 3.83(2)$ for Er^{3+}, which are different from our experimental values. We can also eliminate Sm^{3+} ions, which possess only two isotopes with $I = 7/2$ and which should give a hyperfine pattern in the EPR spectra since the hyperfine A_J constant is around 200 MHz [17]. We are thus left with Ce^{3+} (f^1), Dy^{3+} (f^9) and Yb^{3+} (f^{13}) ions. When the temperature increases between 4.6 and 16 K (figure 7), the intensity of the $Yb_{IIa,IIb}$ lines increases. This indicates that at low temperature a saturation broadening of the transition occurs. This saturation disappears by increasing the temperature due to the rapid decrease of the spin–lattice relaxation time T_1. At 16 K, the $Yb_{IIa,IIb}$ EPR signal looks very similar to that of Yb_I with an identical hyperfine pattern flanking the central line of the spectrum (figure 7). We may thus eliminate the Ce^{3+} ions, which do not present any hyperfine pattern. Moreover, due to this signal shape and as the Dy^{3+} ions are not known to be impurities of Yb^{3+} ions, we can also eliminate this rare earth ion. Finally, the lines referred to as $Yb_{IIa,IIb}$ represent a

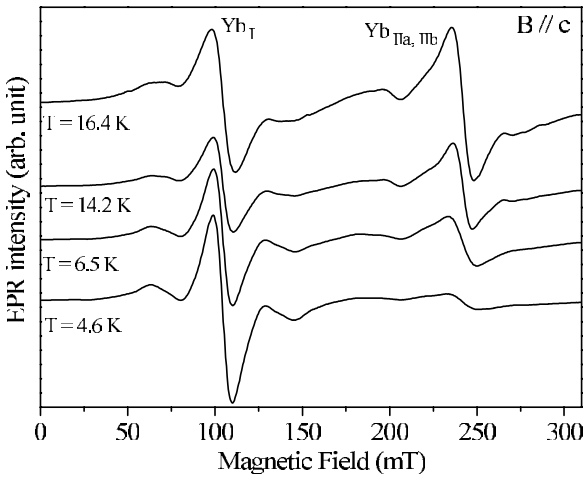

Figure 7. EPR spectrum of the 5% Yb doped $LuVO_4$ crystals as a function of the temperature with the magnetic field parallel to the c axis. The spectra are recorded at 9.5 GHz with a microwave power of 20 mW.

fraction of Yb^{3+} ions localized in two axial sites different from the main Yb_I site. By double integration, we find that these sites correspond to 20% of the Yb^{3+} ions for the 1% doped compound and to 50% of the Yb^{3+} for the 5% doped compound.

In figure 5, we report the experimental g-values of the $Yb_{IIa,IIb}$ sites. The g-factors associated with $Yb_{IIa,IIb}$ do not coincide with the Γ_7 wavefunction but rather with the Γ_6 representation. The g-values are calculated to be $|g_\perp| = 1.05$ and $|g_\parallel| = 3.26$ for Yb_{IIa} and $|g_\perp| = 1.02$ and $|g_\parallel| = 3.27$ for Yb_{IIb} using equation (8) with $|p| = 0.1347$ and $|q| = 0.9910$ and $|p| = 0.1306$ and $|q| = 0.9914$, respectively. This type of wavefunction has already been obtained for Yb^{3+} ions in zircon-structure orthophosphate compounds [25], in a series of scheelite type compounds [24–26], in cubic CaF_2 [27], and in the zircon type silicate $ThSiO_4$ [23]. The discrepancies between the calculated g-values and the experimental one, 20% for Yb_{IIa} and 15% for Yb_{IIb}, could be explained by the existence of covalent bonding [18] and orbit–lattice interaction [19]. However, at maximum, these effects can only explain 5% of the discrepancy. This means that probably mixing by the crystal field of the $J = 5/2$ state into the ground state has to be considered; the wavefunction then has the following form: $|\pm\rangle = p\left|\frac{7}{2}, \pm\frac{5}{2}\right\rangle + q\left|\frac{7}{2}, \mp\frac{3}{2}\right\rangle + r\left|\frac{5}{2}, \pm\frac{5}{2}\right\rangle + s\left|\frac{5}{2}, \mp\frac{3}{2}\right\rangle$. The J-mixing could reduce the discrepancy by nearly 10%. For example, for Yb^{3+} ions in the scheelite type $BaWO_4$ compound [24], when the J-mixing is considered the $g_\parallel$ values increase by about 7%.

The peak-to-peak linewidth Γ of the $Yb_{IIa,IIb}$ central line versus the reciprocal temperature is shown in figure 8 with the magnetic field parallel to the c axis. In the 4.6–16 K temperature range, the linewidth decreases as the temperature increases. This indicates a saturation broadening of the transition at low temperature. In the 16–25 K range, the linewidth increases with the temperature and these variations can be simulated by an Orbach process using equation (11) with a constant inhomogeneous linewidth $A = 11(1)$ mT, $\Delta E = 170(50)$ cm^{-1} and $C = 0.57(5)$ mT/cm^{-3} (figure 8).

3.3. EPR signal referred to Yb_{III}

One set of very weak lines, hereafter referred to as Yb_{III}, are seen at low field around 200 mT when the magnetic field is in the (001) plane (figure 2). These EPR signals are composed of a

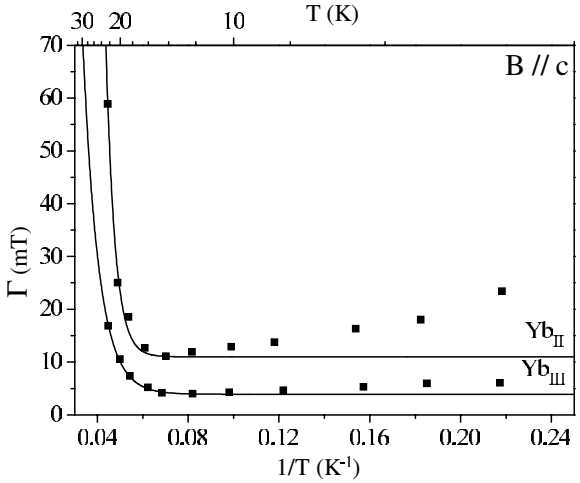

Figure 8. Temperature dependence of the peak-to-peak linewidth Γ of the Yb_{II} and Yb_{III} EPR lines with the magnetic field parallel to the *c* axis. The solid curves are calculated with an Orbach process.

central line and of a hyperfine pattern of two sets of two and six lines with relative intensities proportional to the natural abundances of the two odd isotopes of the ytterbium ions. These transitions attributed to Yb^{3+} ions correspond to less than 1% of the total Yb^{3+} incorporated in the $LuVO_4$ host. In the (100) and (010) planes, an important portion of the angular variation has no experimental data because the EPR transitions are too weak and are hidden by the intense Yb_I EPR lines (figure 3). As it is not possible to follow and to obtain enough experimental values to simulate in three orthogonal planes the angular variations of this signal, we could not build up the *g*-matrix of equation (2) and calculate the principal *g*-values and the cosine director of the principal axes of the tensor. However, we can retrieve several pieces of information from the angular variations. When the magnetic field is rotated in the (001) plane (figure 3), the two lines which compose the Yb_{III} site have exactly the same angular variations with the same values of the extrema but shifted by 90°. This indicates that these two lines correspond to ytterbium ions in the same crystallographic site which are magnetically inequivalent in the (001) plane. The value of 90° shows the presence of a twofold symmetry axis. When the magnetic field is in the (100) or (010) planes (figure 3), each of the previous two lines splits into two other magnetically inequivalent lines. This behaviour can only be seen for the transitions with a high *g*-value (see the experimental points in figure 3) as the other one is hidden by the signal associated with Yb_I and $Yb_{IIa,IIb}$. These magnetic inequivalences reveal that the ytterbium ions associated with these transitions are located in sites with symmetry lower than D_{2d}. This type of site has been already seen in the zircon-type host YMO_4 (M = V, P, As) doped with neodymium ions [11]. In the yttrium compounds, distorted sites with C_{2v} or D_2 symmetry have been observed. These sites present the same kind of magnetic inequivalences when the magnetic field is rotated in the (001), (010) and (100) planes. We can thus conclude that Yb_{III} signals are due to ytterbium ions located in lutetium sites with a low C_{2v} or D_2 point symmetry distorted by the presence of a neighbouring defect such as an impurity.

The peak-to-peak linewidth Γ of the Yb_{III} central line versus the reciprocal temperature is shown in figure 8 with the magnetic field parallel to the *c* axis. The linewidth presents the same behaviour as that of $Yb_{IIa,IIb}$ sites with temperature variations in the 16–25 K temperature

range which can be simulated by an Orbach process with a constant inhomogeneous linewidth $A = 3.9(1)$ mT, an energy splitting $\Delta E = 100(20)$ cm^{-1} and $C = 0.0086(6)$ mT/cm^{-3}.

4. Conclusion

EPR study of Yb^{3+} ions in $LuVO_4$ shows that this ion mainly occupies sites with D_{2d} symmetry. Two kinds of axial site have been observed: Yb_I sites with $|g_\perp| = 0.59(7)$ and $|g_\parallel| = 6.464(9)$ characterized by a wavefunction of the type $p\left|\frac{7}{2}, \pm\frac{7}{2}\right\rangle + q\left|\frac{7}{2}, \mp\frac{1}{2}\right\rangle$ which corresponds to 80% (50%) of the total Yb^{3+} concentrations for the 1% (5%) doped compound; $Yb_{IIa,IIb}$ sites with $|g_\perp| = 0.89(3)$, $|g_\parallel| = 2.75(1)$ for Yb_{IIa} and $|g_\perp| = 0.89(3)$, $|g_\parallel| = 2.84(1)$ for Yb_{IIb} characterized by wavefunctions of the type $p\left|\frac{7}{2}, \pm\frac{5}{2}\right\rangle + q\left|\frac{7}{2}, \mp\frac{3}{2}\right\rangle + r\left|\frac{5}{2}, \pm\frac{5}{2}\right\rangle + s\left|\frac{5}{2}, \mp\frac{3}{2}\right\rangle$ which represent 20% (50%) of the total number of Yb^{3+} in the 1% (5%) Yb-doped compound.

A small fraction of Yb^{3+} ions, less than 1%, are located in sites with low D_2 or C_{2v} symmetry, which are probably distorted lutetium sites with the presence of a neighbouring defect or impurity.

For each site, the study of the spin–lattice relaxation time as function of the temperature indicates a dominant Orbach process for $T > 12$ K.

The presence of three distinct sites is expected to influence the optical spectroscopy and the laser properties of this crystal, as observed in the case of the nonlinear laser crystal $YAl_3(BO_3)_4$:Yb^{3+} [28]. Further investigations of optical spectroscopy of the lutetium compound are under progress.

Acknowledgment

The authors thank E Viviani (University of Verona) for expert technical assistance.

References

[1] Deshazer L 1994 *Laser Focus World* (Tulsa: PennWell Corporation) p 88
[2] Petit J, Viana B, Goldner P, Vivien D, Loiseau P and Ferrand B 2004 *Opt. Lett.* **29** 833
[3] Kränkel C, Fagundes-Peters D, Fredrich S T, Johannsen J, Mond M, Huber G, Bernhagen M and Uecker R 2004 *Appl. Phys.* B **79** 543
[4] Gaumé R, Viana B, Vivien D, Roger J P and Vivien D 2003 *Appl. Phys. Lett.* **83** 1355
[5] Sarukura N, Dubinskii M A, Liu Z, Semashko V V, Naumov A K, Korableva S L, Abdulsabirov R Y, Edamatsu K, Suzuki Y, Itoh T and Segawa Y 1995 *IEEE J. Sel. Top. Quantum Electron.* **1** 792
[6] Laroche M, Girard S, Moncorgé R, Bettinelli M, Abdulsabirov R and Semashko V 2003 *Opt. Mater.* **22** 147
[7] Maunier C, Doualan J L, Moncorgé R, Speghini A, Bettinelli M and Cavalli E 2002 *J. Opt. Soc. Am.* B **19** 1794
[8] Barnes N P 1995 *Solid State Lasers and Nonlinear Crystals* (*Proc. SPIE* vol 2379) ed G J Quarles, L Esterowitz and L K Cheng (Bellingham, WA: SPIE Optical Engineering Press) p 2
[9] Dujardin C, Pedrini C, Gâcon J C, Petrosyan A G, Belsky A N and Vasil'ev A N 1997 *J. Phys.: Condens. Matter* **9** 5229
[10] Chakoumakos B C, Abraham M M and Boatner L A 1994 *J. Solid State Chem.* **109** 197
[11] Guillot-Noël O, Simons D and Gourier D 1999 *J. Phys. Chem. Solids* **60** 555
[12] Guillot-Noël O, Viana B, Bellamy B, Gourier D, Zogo-MBoulou G B and Jandl S 2000 *Opt. Mater.* **13** 427
Jandl S, Guillot-Noël O and Gourier D 2002 *Opt. Mater.* **19** 449
[13] Abraham M M, Bleaney B and Pfeffer J Z 1998 *Appl. Magn. Reson.* **14** 393
[14] Garton G, Smith S H and Wanklyn B M 1972 *J. Cryst. Growth* **13/14** 588
[15] Dabrowski A, Dabrowska H and Jasiolek G 1985 *J. Less-Common Met.* **110** 255
[16] Mabbs F E and Collison D 1992 *Electron Paramagnetic Resonance of d Transition Metal Compounds* (*Studies in Inorganic Chemistry* vol 16) (New York: Elsevier)
[17] Abragam A and Bleaney B 1986 *Electron Paramagnetic Resonance of Transition Ions* (New York: Dover)
[18] Bleaney B 1964 *Proc. R. Soc.* A **277** 289

[19] Inoue M 1963 *Phys. Rev. Lett.* **11** 196
[20] Reynolds R W, Boatner L A, Chen Y and Abraham M M 1974 *J. Chem. Phys.* **60** 1593
[21] Abraham M M, Finch C B, Kolopus J L and Lewis J T 1971 *Phys. Rev.* B **3** 2855
[22] Ranon U 1968 *Phys. Lett.* A **28** 228
[23] Reynolds R W, Boatner L A, Finch C B, Châtelain A and Abraham M M 1972 *J. Chem. Phys.* **56** 5607
[24] Sattler J P and Nemarich J 1970 *Phys. Rev.* B **1** 4249
[25] Abraham M M, Boatner L A, Ramey J O and Rappaz M 1983 *J. Chem. Phys.* **78** 3
[26] Sattler J P and Nemarich J 1971 *Phys. Rev.* B **4** 1
[27] Kirton J and McLaughlan D 1967 *Phys. Rev.* **155** 279
[28] Ramírez M O, Bausá L E, Jaque D, Cavalli E, Speghini A and Bettinelli M 2003 *J. Phys.: Condens. Matter* **15** 7789